

Learn to Position - A Novel Meta Method for Robotic Positioning

Dongkun Wang^{*†}, Junkai Zhao[§], Yunfei Teng^{‡¶}, Jieyang Peng^{*†}, Wenjing Xue[‡], Xiaoming Tao ^{*†||}

^{*}Department of Electronic Engineering, Tsinghua University, Beijing 100084, P.R.China

[†]Beijing National Research Center for Information Science and Technology

[§]Department of Mechanical and Automation Engineering, The Chinese University of Hong Kong

[‡]Department of Mechanical Engineering, Tongji University, Shanghai, China

Abstract—Absolute positioning accuracy is a vital specification for robots. Achieving high position precision can be challenging due to the presence of various sources of errors. Meanwhile, accurately depicting these errors is difficult due to their stochastic nature. Vision-based methods are commonly integrated to guide robotic positioning, but their performance can be highly impacted by inevitable occlusions or adverse lighting conditions.

Drawing on the aforementioned considerations, a vision-free, model-agnostic meta-method for compensating robotic position errors is proposed, which maximizes the probability of accurate robotic position via interactive feedback. Meanwhile, the proposed method endows the robot with the capability to learn and adapt to various position errors, which is inspired by the human’s instinct for grasping under uncertainties. Furthermore, it is a self-learning and self-adaptive method able to accelerate the robotic positioning process as more examples are incorporated and learned. Empirical studies validate the effectiveness of the proposed method. As of the writing of this paper, the proposed meta search method has already been implemented in a robotic-based assembly line for odd-form electronic components.

Index Terms—Deep Learning in Robotics and Automation, Force and Tactile Sensing, Learning and Adaptive Systems, Robotic Positioning

I. INTRODUCTION

Recent studies have witnessed significant advancements in robotic automation, including applications such as robotic assembly [1], robotic gridding [2], and robotic intervention [3] [4]. Accurate robotic positioning is a prerequisite for these applications. Robotic positioning errors can be broadly categorized as *internal errors* and *external errors* [5]. Internal errors arise from factors such as joint and link compliance or gear backlash associated with the robot. On the other hand, external errors result from factors in the robot’s external environment, such as inaccurate tool and fixture positions. Therefore, developing an effective method to compensate for positioning deviations resulting from internal and external errors is crucial. To enhance the accuracy of robotic positioning, auxiliary devices, for example, positioners, have been developed to guide the robotic end effector to the desired point with increased precision [6]. Nonetheless, these auxiliary devices are typically designed for a specific task and are not easily adaptable to other tasks, which limits their versatility.

The vision-based robotic positioning mainly involves capturing visual data through a camera, which can provide either

2D or 3D information, and subsequently leveraging this information to infer the object’s geographical location [7]. Although numerous studies have focused on enhancing the position accuracy of vision-based position control [8] [9], this approach inherently suffers from limitations, e.g., unexpected occlusions or poor lighting conditions. Given the challenges in accurately depicting positioning errors, artificial neural networks offer a viable solution for compensating the absolute positioning errors [10] [11]. The performance of neural networks is highly dependent on the quality of training data, which is difficult to acquire from real-world robotic environments. The structure and parameters of neural networks significantly impact their performance. Therefore, it is a challenging task to construct a neural network that can effectively generalize to various position errors encountered in real-world scenarios. In complicated robotic applications(e.g., robotic assembly), the trained neural network may not effectively generalize to new tasks without fine-tuning.

In complicated robotic applications, e.g., robotic assembly in a cluttered environment, occlusions between manipulated objects can influence the end-effector’s positioning ability. Considering the vision’s inherent limitations in occlusions, a vision-free positioning method is proposed. The robotic positioning problem is first comprehensively addressed from a statistical standpoint by formulating it as a probability maximization task via sampling from a Gaussian distribution, which is consistent with the principles of the law of large numbers, resulting in a complete and effective solution. A numerical method adapted from the Monte Carlo method is proposed to improve sampling accuracy, which serves to approximate the integral. To evaluate the effectiveness of the proposed method, printed circuit board (PCB) assembly was chosen as the study case, where the robot assembles a set of non-standard odd-form electronic components onto the PCBs.

The main contributions of this work are listed as follows:

- (1) **Design of a novel self-adaptive meta search method for robotic positioning.** The *meta*-method involves two key steps: (a) updating the fitted posterior of the Gaussian distribution, (b) maximizing the rate of successful sampling based on the modeled distribution. The probability of the accurate position will be maximized through interactive feedback.
- (2) **Design of an automated assembly facility for odd-form electronic components.** The automatic assembly equipment for odd-form electronic components was designed to enable

[¶] Meta method design and corresponding author

^{||} Contact author for remaining sections

the assembly of various types of odd-form electronic components. Collaborative robots are utilized for the assembly. A special gripper has been designed to ensure the smooth clamping of odd-form electronic components.

(3) Empirical study of the proposed method. An empirical study of the assembly efficiency is conducted with IGBT as the experimental object. The experimental results indicate that, the proposed meta search method achieves superior assembly efficiency compared with other methods, meanwhile possessing the best self-adaption ability.

II. RELATED WORK

Over the past few years, there has been a growing trend in using visual sensors in robotic positioning systems. As the technology of visual sensors continues to mature, the cost of these sensors has become increasingly affordable. By utilizing visual sensors, valuable information regarding the shape, stripes, color, and relative position of objects can be obtained [12]. Subsequently, the end-effector can be servoed to the position obtained from the visual information.

Gregorio et.al [13] developed a manipulation system for electric wires insertion. The synergy between computer vision and tactile sensing enables wires to be precisely positioned by the robot in tight insertion spaces. A technique for inserting an elastic flexible wire into a hole while utilizing stereo vision to observe the wire's shape was introduced by Nakagaki et al. [14]. Feng et al. [15] introduced a sub-centimeter-level metrology system based on computer vision, which utilizes planar markers to facilitate pose estimation for construction robots. Qin et al. [16] presents a novel assembly system for large-scale objects that utilizes two cameras and three laser distance sensors to achieve precise object assembly. However, achieving high-precision object assembly necessitates the introduction of multiple sensors, such as cameras and lasers, which can lead to high hardware costs. Wan et al. [17] use multi-modal 3D vision to deduce object positions during assembly. While this approach addresses the issue of imprecise 3D visual detection, it requires the attachment of AR markers to the objects beforehand. Chang [18] proposed a vision-based control method for the automatic assembly of smartphone back shells. Calibrated binocular vision can be utilized to reconstruct the 3-D positions and normal vectors of both the phone and its back shell.

Cheng et al. [19] proposed to utilize an uncalibrated vision system mounted on another robot to teach the robot precise assembly, thus decreasing the robot position errors in unstructured environments. Nonetheless, the addition of another robot results in a no longer cost-effective assembly system. Fontana [20] designed an experimental setup based on 4 degrees of freedom robot and a two-camera vision system. A portable and flexible program was developed in which a machine vision module incorporates a control module for task operation. Lin [21] developed a machine vision-based electronic component insertion system with cooperative dual SCARA, taking advantage of multiple robots with a compact structure, higher flexibility, and higher productivity. Zhang [22] presents a locating method that combines traditional threshold segmentation, feature information extraction, and edge contour

fitting to detect and locate electronic components and PCB holes. The deviation in the edge unsmoothness caused by the initial edge contour is solved using an edge contour fitting technique. Liang [23] proposes a novel position correction method for the electronic components' auto-insertion based on rotational stereo vision. A four-degree-of-freedom auto-insertion system based on rotational stereo vision is set up. Then, the rotational stereo vision system detects the electronic component's pose. Liu [24] introduced a robust method that combines image enhancement, edge detection, and feature information extraction to detect and locate target components. The key idea is to use a histogram key point constrained homomorphic filtering to enhance the image followed by line and arc segments feature detection. Nerakae [25] integrated the machine vision system with the robotic system to conduct a pick-and-place process. When the main parts were held at a specific location, the images of the main parts were captured. Using the image processing of LabVIEW NI vision software and NI vision builder and image calibration method, the author could obtain the shape and orientation of assembling space in the main part, which were used to control selective compliance articulated robot arm (SCARA).

Although vision systems have become a primary source of feedback in robotics due to their ability to provide detailed position information, the reliability of the location output from the vision system may be compromised due to camera calibration deviation. Additionally, vision systems can be challenging to apply when objects are visually confused or occluded. Furthermore, the deployment of increasingly intricate vision systems can prove to be cost-prohibitive.

III. METHODOLOGY

A. Problem Statement

The emphasis is on addressing position errors in robots employed for assembly tasks. This study commences with establishing a mathematical model and a rigorous explanation of the algorithms. Subsequently, the proposed methodology is applied in the robot assembly scenario to evaluate its effectiveness in addressing position errors.

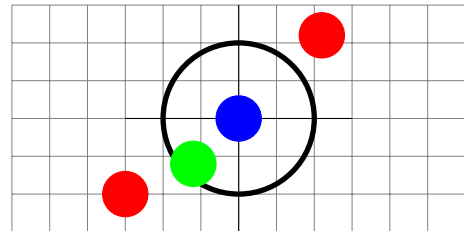


Fig. 1. Cases of component insertion. **Blue circle**: feasible; **Red circle**: not feasible; **Green circle**: on the boundary.

The robot assembly process involves retrieving an object by the robot and its subsequent insertion into another object at a predetermined position. As depicted in Fig. 1, the enclosed largest black circle represents the feasible area around the insertion point (center of the largest). The object can be successfully assembled when inserted in the feasible area.

It should be noted that each attempt to assemble the components may result in a slightly different feasible insertion area. Thus the center of the feasible area as a random variable \mathbf{a} and the radius of that area as a random variable \mathbf{b} , which could be assumed as both random variables with bounded mean and variance (i.e., $\|a\| + \|b\| < +\infty$) are considered. In short, the distribution of the feasible area c could be represented as:

$$\mathbf{c} = \mathbf{a} + \mathbf{b} \quad \mathbf{a} \sim \mathcal{N}(\mu_a, \Sigma_a), \mathbf{b} \sim \mathcal{N}(\mu_b, \Sigma_b) \quad (1)$$

where \mathbf{c} is a random variable as well. For the sake of simplicity, both a and b are assumed as Gaussian random variables. Consequently, c is a Gaussian random variable as well. In our following analysis, only one Gaussian distribution random variable is considered.

Proof. The characteristic function of a multidimensional random variable is defined as the Fourier transform of its joint probability density function (PDF). Let's denote the multidimensional random variable as $\mathbf{X} = (X_1, X_2, \dots, X_n)$, where n is the number of dimensions. The characteristic function of \mathbf{X} , denoted as $\phi(\mathbf{t})$, is defined as:

$$\phi(\mathbf{t}) = E[e^{i\mathbf{t} \cdot \mathbf{X}}]$$

where $\mathbf{t} = (t_1, t_2, \dots, t_n)$ is a vector of parameters, $\mathbf{t} \cdot \mathbf{X}$ represents the dot product of the vectors \mathbf{t} and \mathbf{X} , and i is the imaginary unit.

The characteristic function of the sum of two independent random variables X and Y is just the product of the two separate characteristic functions $\varphi_{X+Y}(t) = E[e^{i\mathbf{t} \cdot (\mathbf{X} + \mathbf{Y})}]$ of the sum of two independent random variables X and Y is just the product of the two separate characteristic functions:

$$\varphi_X(t) = E[e^{i\mathbf{t} \cdot \mathbf{X}}], \quad \varphi_Y(t) = E[e^{i\mathbf{t} \cdot \mathbf{Y}}]$$

of X and Y . The characteristic function of the normal distribution with expected value μ and Σ

$$\varphi(t) = \exp\left(it^T \mu - \frac{t^T \Sigma t}{2}\right).$$

Thus

$$\varphi_{X+Y}(t) = \varphi_X(t) \cdot \varphi_Y(t) \quad (2)$$

$$= \exp\left(it^T \mu_X - \frac{t^T \Sigma_X t}{2}\right) \exp\left(it^T \mu_Y - \frac{t^T \Sigma_Y t}{2}\right) \quad (3)$$

$$= \exp\left(it^T (\mu_X + \mu_Y) - \frac{t^T (\Sigma_X + \Sigma_Y) t}{2}\right). \quad (4)$$

This is the characteristic function of the normal distribution with expected value $\mu_X + \mu_Y$ and covariance matrix $\Sigma_X + \Sigma_Y$.

Finally, recall that no two distinct distributions can both have the same characteristic function, so the distribution of $X + Y$ must be just this normal distribution. \square

The goal is to insert each object into the appropriate area successfully with minimal attempts. The possibility of each attempt falling into the circle of the feasible area is being maximized, which in turn leads to the maximization of the

integral problem. To be more specific, assuming that n times and for i^{th} attempt can be performed, the tolerance is ϵ_i centered at x_i . Let D_i be the circle of radius ϵ_i centered at the x_i and the following equation will be resolved:

$$\max \int_{\cup_{i=1}^n D_i} f_c(y) dy \quad (5)$$

where $f_c(y)$ is the probability distribution of \mathbf{c} at point y . The union operator is used instead of summation, as repeated sampling at the overlapping area is avoided.

B. Algorithmic-based Search Method

This section commences by presenting several search methods characterized by a predefined sampling trajectory and a termination criterion based on the successful execution of the insertion task.

1) *Linear search:* The basic principle of the linear search method is that the robot will implement a linear search process along a straight search line to determine the hole position. The linear search method comes from the work by Chhatpar [26] and has been modified to better suit PCB assembly requirements. The linear search method introduces a linear motion along a defined search line starting from the robot's predefined insertion position. The end-effector gripping a component will move to the predefined insertion position during the insertion process and implement the insertion step. If the robot can successfully insert the component into the hole, the robot will not implement the linear search method. If the robot can not insert the peg, the end-effector will move along a search line at a concrete distance to get to a new insertion position. The robot will then execute the insertion action from that new insertion position. As the actual hole could locate randomly at the search line, the predefined insertion position is set as the central point of the search line. Theoretically, the actual insertion position could locate uniformly at either side of the central point. Therefore, the search positions locate at either side of the central point and follow a uniform distribution. The end-effector moves in reverse search directions within two continuous search cycles, respectively, which ensures that both directions of the predefined insertion position can be searched. The linear search process will be terminated upon successfully inserting the component into the hole or upon reaching the maximum allotted search cycle.

During the search process, the end-effector gripping the component moves along a certain search line l . In the i -th insertion cycle, the insertion position $P_i(x_i, y_i, z)$ follows:

$$x_i = x_{i-1} + s \cdot i \cdot (-1)^i \cdot \cos \theta \quad (6)$$

$$y_i = y_{i-1} + s \cdot i \cdot (-1)^i \cdot \sin \theta \quad (7)$$

where θ means the angle between the search line l and the X axis of the robot base coordinate. The present study focuses on the assembly process in a two-dimensional plane, where the z element of the insertion position remains constant for all the insertion positions. $P_0(x_0, y_0, z)$ is the predefined insertion position. The insertion process is simplified through omitting the rotation movement of the peg. The concrete distance

between two successive insertion points is stride s , and the maximal search cycle is m .

2) *Spiral search*: The end-effector's path during the spiral search process [27] is the *Archimedean spiral*. The spiral search method is employed if the robot cannot insert the component at the predefined insertion position. In the spiral search process, the end-effector executes an Archimedean spiral motion originating from the predefined insertion position. This motion continuously expands outward on the XY plane. During each search step, the maximal search radius of the Archimedean spiral is r . Given P_0 , the angular change between two successive insertion cycles is θ_d , the cumulative angular search range θ_{mx} is defined as:

$$\theta_{mx} = t \cdot 360^\circ \quad (8)$$

where t is the total turns of the spiral. The per-degree change in radius r_d is :

$$r_d = \frac{r}{\theta_{mx}} \quad (9)$$

In the i -th insertion cycle, the accumulated degrees the peg has obtained from the start of search implementation θ_{cur} is:

$$\theta_{cur} = \theta_d \cdot i \quad (10)$$

The current radius r_{cur} of the i -th search point on the spiral is calculated as:

$$r_{cur} = \theta_{cur} \cdot r_d \quad (11)$$

The i -th insertion position $P_i(x_i, y_i, z)$ is updated using the following equation:

$$x_i = x_0 + r_{cur} \cdot \cos \theta_{cur} \quad (12)$$

$$y_i = y_0 + r_{cur} \cdot \sin \theta_{cur} \quad (13)$$

During the spiral search process, the robot with its compliant feature consistently exerts a slight force in the $-Z$ direction to the component. The exerted force enables the component to be instantly inserted into the hole when the component moves over the hole. Similarly to the linear search method, the spiral search process is terminated upon successfully inserting the component into the hole or reaching the maximum search radius defined by r .

3) *Hybrid search*: The drawback of the linear search method is that only when the target hole located on the search line will be reached successfully, while the hole deviating from the search line will not. The robot must conduct tedious search cycles step by step when the hole does not locate at the search line, which is time-consuming and inefficient. What is worse, the robot could not insert the component even though the hole is near the search line.

Compared with the linear search method, the search areas using the spiral search method are more extensive, which means that the spiral search method is more reliable for search dispersively distributed holes. Despite that, the search area is constrained in a limited area. The robot utilizing the spiral search method can fail to insert the component when the hole locates far from the predefined insertion position. Therefore, a hybrid search method that could balance the drawbacks of these two search strategies should be developed. The hybrid

search method consists of linear and spiral search strategies. The robot will first implement one cycle of the linear search motion. The spiral search motion will be immediately implemented when the component cannot be inserted due to various tolerances. Algorithm 1 illustrates the complete hybrid search method.

Algorithm 1 Hybrid search method

Require: predefined insertion position

```

while component not inserted do
  searchmode  $\leftarrow$  linear search
  if component is inserted then
    search mode  $\leftarrow$  search break
  else if component is not inserted then
    search mode  $\leftarrow$  spiral search
  end if
end while
return acutal insertion position

```

C. Meta search

The aforementioned search method cannot be adjusted flexibly, meanwhile these methods cannot learn useful information from the previous samples taken advantage of at all. As a result, a new meta search method that iteratively update the status of the learning model to speed up insertion processes is proposed.

The model is in principle divided into two stages: (1) A prior of the distribution is firstly defined, and the posterior will be updated recursively, and (2) a search method that is based on gradient ascent is introduced. Based on the Gaussian distribution assumption, such an update could be done recursively, meaning these two steps will be done alternately.

1) *Gaussian Distribution*: The formula for a two-dimensional Gaussian function [28] in matrix form is as follows [29]:

$$f(\mathbf{x}) = \frac{1}{\sqrt{2\pi}|\Sigma|} \exp\left(-\frac{1}{2}(\mathbf{x} - \boldsymbol{\mu})^T \Sigma^{-1}(\mathbf{x} - \boldsymbol{\mu})\right)$$

In this formula, \mathbf{x} represents the vector of variables (x, y) , $\boldsymbol{\mu}$ denotes the mean vector (μ_1, μ_2) , Σ represents the covariance matrix:

$$\Sigma = \begin{bmatrix} \sigma_1^2 & \rho\sigma_1\sigma_2 \\ \rho\sigma_1\sigma_2 & \sigma_2^2 \end{bmatrix}$$

Here, σ_1 and σ_2 represent the standard deviations in the x and y directions, respectively, and ρ denotes the correlation coefficient between the x and y variables.

2) *Distribution Update*: The problem could be easily solved by using *Maximum Likelihood Estimation* (MLE) or *Maximum a Posterior* (MAP). Firstly, it is noteworthy that a likelihood function could be expressed as

$$\hat{\theta}_{MLE}(x) = \arg \max_{\theta} f(x | \theta)$$

while a posterior could be given by

$$\hat{\theta}_{MAP}(x) = \arg \max_{\theta} f(x | \theta) = \arg \max_{\theta} f(x|\theta)g(\theta)$$

For Gaussian distribution, there is a closed-form solution for estimation. The logarithm of Gaussian distribution is taken and the results are obtained as follows:

$$\log f(\mu, \Sigma; x) = -\frac{1}{2} \log |\Sigma| - \frac{1}{2} (x - \mu)^T \Sigma^{-1} (x - \mu) \quad (14)$$

$$\frac{\partial}{\partial \mu} \log f(\mu, \Sigma; x) = -\Sigma^{-1} (x - \mu) \quad (15)$$

$$\frac{\partial}{\partial \Sigma^{-1}} \log f(\mu, \Sigma; x) = -\frac{1}{2} \Sigma - \frac{1}{2} (x - \mu)(x - \mu)^T \quad (16)$$

By setting the gradient to zeros, the result comes up with

$$\hat{\mu} = \frac{1}{m} \sum_{i=1}^m x_i, \quad \hat{\Sigma} = \frac{1}{m} \sum_{i=1}^m (x_i - \hat{\mu})(x_i^T - \hat{\mu})^T \quad (17)$$

Notice that MLE is a biased estimation for the con-variance matrix, but in practice it does not make too much difference as the number of data points increases. To solve for MAP, assuming that each element of both μ and Σ is given a prior of Gaussian distribution $\mathcal{N}(0, 1)$, then equations 14, 15 and 16 become

$$\begin{aligned} \log f(\mu, \Sigma; x) &= -\frac{1}{2} \log |\Sigma| - \frac{1}{2} (x - \mu)^T \Sigma^{-1} (x - \mu) \\ &\quad - \frac{\lambda_1}{2} \cdot \|\mu - \tilde{\mu}\|_2^2 - \frac{\lambda_2}{4} \cdot \|\Sigma - I\|_2^2 \end{aligned} \quad (18)$$

$$\frac{\partial}{\partial \mu} \log f(\mu, \Sigma; x) = -\Sigma^{-1} (x - \mu) - \lambda_1 (\mu - \tilde{\mu}) \quad (19)$$

$$\frac{\partial}{\partial \Sigma^{-1}} \log f(\mu, \Sigma; x) = -\frac{1}{2} \Sigma - \frac{1}{2} (x - \mu)(x - \mu)^T - \frac{\lambda_2}{2} (\Sigma - I) \quad (20)$$

And

$$\hat{\mu} = (I + \lambda_1 \Sigma)^{-1} \left(\frac{1}{m} \sum_{i=1}^m x_i + \lambda_1 \tilde{\mu} \right), \quad (21)$$

$$\hat{\Sigma} = \frac{1}{1 + \lambda_2} \left(\frac{1}{m} \sum_{i=1}^m (x_i - \hat{\mu})(x_i^T - \hat{\mu})^T + \lambda_2 I \right)$$

For MAP, the estimation can be considered as a regularized parameter optimization problem.

3) *Maximize the probability:* Our goal is to find the integral of

$$\frac{\partial}{\partial m} \int_{x \in U_\epsilon(m)} f(x) dx = \Sigma^{-1} \int_{z \in U_\epsilon(0)} (m + z - \mu) \cdot f(m + z) dz \quad (22)$$

$$\begin{aligned} &= \Sigma^{-1} \int_{z \in U_\epsilon(0)} (m + z) \cdot f(m + z) dz \\ &\quad - \Sigma^{-1} \int_{z \in U_\epsilon(0)} \mu \cdot f(m + z) dz \end{aligned} \quad (23)$$

The first line is by interchanging integration and differentiation. This integral is then solved separately.

$$\int_{z \in U_\epsilon(0)} f(m + z) dz = \int_{x \in U_\epsilon(m)} f(x) dx \quad (24)$$

$$= \frac{1}{2\pi \sqrt{|\Sigma|}} \int_{x \in U_\epsilon(m)} \exp\left(-\frac{1}{2} (\mathbf{x} - \boldsymbol{\mu})^T \Sigma^{-1} (\mathbf{x} - \boldsymbol{\mu})\right) dx \quad (25)$$

$$= \frac{1}{2\pi \sqrt{|\Sigma|}} \int_{x \in U_\epsilon(m)} \exp\left(-\frac{1}{2} (\mathbf{x} - \boldsymbol{\mu})^{-1} T \Lambda T^T (\mathbf{x} - \boldsymbol{\mu})\right) dx \quad (26)$$

$$= \frac{1}{2\pi \sqrt{|\Sigma|}} \int_{y \in U(m-\mu, \epsilon)} \exp\left(-\frac{1}{2} \mathbf{y}^T \Lambda \mathbf{y}\right) |T| dy \quad (27)$$

$$= \frac{1}{2\pi \sqrt{|\Sigma|}} \int_{y \in U(m-\mu, \epsilon)} \exp\left(-\frac{1}{2} \mathbf{y}^T \Lambda \mathbf{y}\right) dy \quad (28)$$

The third line is given by $T^{-1}(x - \mu) = y \Rightarrow dx = T dy$, and the following step is based on the fact that T is an orthogonal matrix. To be more specific, the columns of T are the eigenvectors of Σ , and the diagonal elements of Λ are eigenvalues (i.e., $\Sigma = T \Lambda T^T$). Using a similar trick (or integral by parts), the following equation shall be found

$$\begin{aligned} \int_{z \in U_\epsilon(0)} (m + z) \cdot f(m + z) dz &= \int_{x \in U_\epsilon(m)} x f(x) dx \\ &= \frac{1}{2\pi \sqrt{|\Sigma|}} \int_{y \in U(m-\mu, \epsilon)} (T y + \mu) \exp\left(-\frac{1}{2} \mathbf{y}^T \Lambda \mathbf{y}\right) dy \end{aligned} \quad (29)$$

Bringing everything together gives the following results:

$$\begin{aligned} \frac{\partial}{\partial m} \int_{x \in U_\epsilon(m)} f(x) dx &= \frac{\Sigma^{-1} T}{2\pi \sqrt{|\Sigma|}} \int_{y \in U(m-\mu, \epsilon)} y \exp\left(-\frac{1}{2} \mathbf{y}^T \Lambda \mathbf{y}\right) dy \quad (30) \\ &= \frac{T \Lambda}{2\pi \sqrt{|\Lambda|}} \int_{y \in U(m-\mu, \epsilon)} y \exp\left(-\frac{1}{2} \mathbf{y}^T \Lambda \mathbf{y}\right) dy \quad (31) \end{aligned}$$

The resulting expressions are intractable as the integrals cannot be expressed in terms of elementary functions (one can check that the double integral given in Eq.31 involves a term of error function as the calculation of the cumulative distribution of Gaussian distribution is required). Therefore, it may be more practical to use numerical or computational method to approximate the derivatives rather than attempting to derive them analytically.

By observation, it is found that the relation between $\frac{\partial f(x)}{\partial x}$ and $\frac{\partial f(m+z)}{\partial m}$ subject to the constraint $x = m + z$.

$$\frac{\partial f(\mathbf{x})}{\partial x} = \frac{1}{2} \frac{\partial}{\partial \mu} [(\mathbf{x} - \boldsymbol{\mu})^T \Sigma^{-1} (\mathbf{x} - \boldsymbol{\mu})] \cdot f(\mathbf{x}) \quad (32)$$

$$= \Sigma^{-1} (x - \mu) \cdot f(x) \quad (33)$$

Similarly,

$$\frac{\partial f(\mathbf{m} + \mathbf{z})}{\partial m} = \Sigma^{-1} (m + z - \mu) \cdot f(m + z) \quad (34)$$

Thus, the following formula shall be seen:

$$\frac{\partial}{\partial m} \int_{x \in U_\epsilon(m)} f(x) dx = \int_{x \in U_\epsilon(m)} \frac{\partial f(\mathbf{x})}{\partial x}$$

Algorithm 2 Meta search method

Require: Assign *predefined insertion position* as m_0 and initialize the prior distribution as $\mathcal{N}(m_0, I)$

repeat

Part 1: Maximize the probability

Generate a sequence of candidates by Equation 36 or 37

Sort the candidate by the probabilities of being inserted

while *peg not inserted* **do**

Try next candidate point

end while

Part 2: Distribution Update

Update the posterior distribution based on the new point x_t by Equation 17 or 21.

until All components are successfully inserted

- ▷ generate candidate points for subsequent steps
- ▷ increase the likelihood of successful insertion
- ▷ meet an unsuccessful case and move to next

Next, equation

$$\phi(m; \epsilon) = \int_{x \in U_\epsilon(m)} f(x) dx \quad (35)$$

is defined, which indicates the chance of successfully making insertion. To approximate the integral, the Monte Carlo sampling method could be applied. Furthermore, to obtain the maximal value of $\phi(m)$ in a numerical way and propose a numerical meta method.

Since only two dimensions are involved, the problem "Curse of Dimensionality" in the field of machine learning is not concerned. Furthermore, since the assumed distribution is simple enough, there is no need to implement methods like meta-dynamics to escape the so-called low-energy landscape. Thus Monte Carlo seems to be a good choice.

On the other hand, since it is unnecessary to get a perfect solution and the best solution can be chosen empirically from several trials, the magic idea of gradient descent method can be safely accepted. By combining the gradient descent method with the Monte Carlo method, it is possible to find a cover centered on m that maximizes the value of $\phi(m)$. An example could be found at Fig 2.

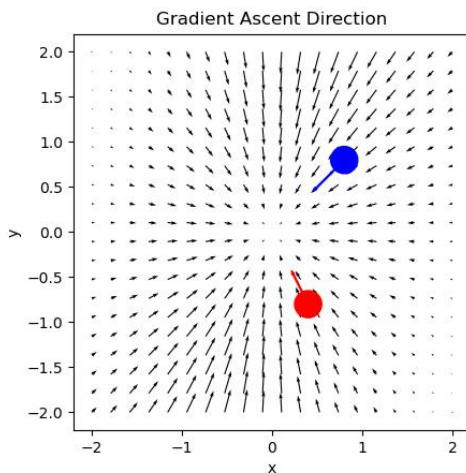


Fig. 2. Gradient ascent direction for the case of two search covers. The black short arrows show the gradient decent directions.

Our the final goal is to find n covers that maximize the probability to insert the components. Therefore, to avoid

collapse of the covers, a repelling force will be exerted to each pair of covers. The objective function is given as follows:

$$\Phi_i(m) = \phi(m_i) + \frac{\lambda}{n-1} \sum_{j \neq i} \max(\|m_i - m_j\|_2^2 - \epsilon, 0) \quad (36)$$

Or equally, the repelling strength between each cover and their center can be added, which yields:

$$\Phi_i(m) = \phi(m_i) + \lambda \cdot \|m_i - \frac{1}{n} \sum_{j=1}^n m_j\|_2^2 \quad (37)$$

In both Eq.36 and Eq.37, the term λ controls the strength that punishes distances between the centers of the covers. By solving the equations introduced, the function F to be maximized is defined as

$$F = \sum_i \Phi_i(\mu) \quad (38)$$

Combining steps (1), (2) and (3), a complete meta search method shown in Algorithm 2 is proposed, which could be extended to any number of expected points for search. In the end, the centers of covers will be found after search and their coordinates will be sent to the robot.

IV. SYSTEM OVERVIEW

This section will introduce the odd-form electronic component assembly, which is error-sensitive to evaluate the robot's positioning ability. In the electronic component assembly process, the printed circuit board (PCB) is initially mounted onto a tray and securely fastened, following which the end effector carries out a series of operations. Firstly, the end effector picks up the electronic component utilizing the fixture. Subsequently, the end effector moves the component to a predetermined insertion position. Finally, the end effector inserts the component into the circuit board, completing the assembly process. The accurate positioning of the electronic component during insertion is of utmost importance, as any inaccuracies can lead to failure. The robot may encounter dynamic constraints or occlusions caused by multiple electronic components previously inserted into the PCB. Moreover, the time required for the insertion process is also crucial, as an excessively long insertion time can render the process impractical. Hence, it is crucial for the robot to perform assembly process with maximum precision and efficiency.

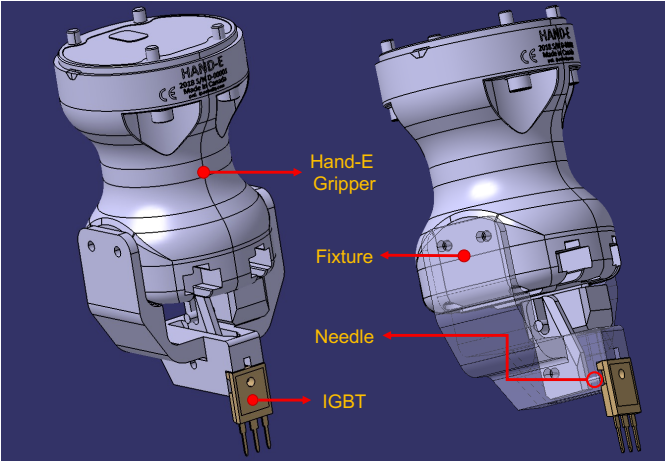


Fig. 3. Illustration of robot gripper(in virtual environment).

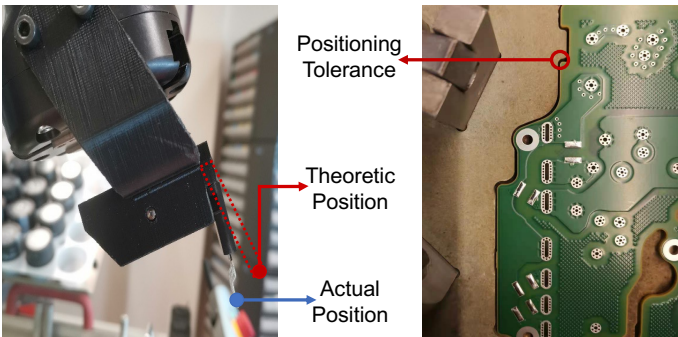


Fig. 4. Examples of components clamping tolerance(left) and positioning tolerance(right) during assembly.

One typical odd-form electronic component, IGBT, is selected to be assembled in PCB. The IGBT's appearance is displayed in Fig 3. This type of component is challenging for automatic assembly, each IGBT possesses three pins and can only be successfully inserted when all three pins are simultaneously inserted into their respective holes. To pick up the IGBT, a 3D-printed fixture mounted on the gripper is developed. The opening and clamping actions of the fixture are achieved by the parallel movement of two sliders on the gripper. During the fixture operation, the sliders move in opposite directions. The pickup mechanism within the fixture completes the component's picking-up action. During the component pickup process, one slider moves in a certain direction, and the fixture controls the slider's movement. Through the pickup mechanism on the gripper, the metal needle rotates along the clamping direction of the IGBT. When the metal needle rotates into the through-hole in the IGBT and clamps it, the slider of the fixture stops moving. When the IGBT is successfully inserted into the circuit board, the slider of the fixture moves in the opposite direction, so the metal needle also rotates in the opposite direction. The metal needle rotates out of the through-hole and releases the IGBT.

The primary factor that impacts the precision of the assembly is the range of tolerances involved. Various tolerances affect the robot's position ability in the assembly process. For example, shape tolerance arises from the blending of

the pin due to its low stiffness, while component clamping tolerance arises when the fixture fails to clamp the component accurately. Additionally, the PCB's manufacturing tolerance and the tray's position tolerance can also affect the hole's position on the PCB. An example of components clamping tolerance and PCB position tolerance is shown in Fig 4.

A tolerance-adaptive assembly method will be developed to handle the various tolerances listed above. The paper focuses on the adaptive positioning problem during the assembly process. The basic principles involved are as follows. Upon grasping an IGBT, the robot moves it to the predetermined insertion position and proceeds to perform the insertion operation. The initial insertion of the IGBT is likely to fail due to various tolerances. When pins of the IGBT cannot be inserted into the circuit board, there is a reaction force between the electronic pins and the circuit board, according to which the robot determines whether the components are successfully assembled through the integrated force sensor. In case of an assembly failure, the robotic system will responsively initiate a search process near the intended insertion position. Analogous to the fine-tuning in the manual assembly process, the robot will explore the actual insertion positions until the IGBT's pins are inserted into the mounting holes. The coordinates of the successful assembly position will be recorded in the system.

V. EXPERIMENT

A. Experiment Configuration

The search method is implemented on a Universal Robot 3e (UR3e). The UR robot is embedded into a flexible assembly unit [30](see Fig.6). The assembly unit is equipped with a safety light curtain *miniTwin4* for safe interaction with operators during assembly. If a human enters the robot's working area, the light curtain is triggered, which subsequently halts the robot's operation. In case that the IGBT cannot be successfully inserted into its corresponding holes after reaching the maximum allotted search cycles, human intervention is required to halt the assembly process. A bare PCB is placed on a carrier for each assembly cycle. The carrier, along with the PCB, is transported to the assembly unit via conveyors. In each cycle, the robot picks up a single IGBT and moves it to the initialized insertion position. At this point, one of the search methods is selected, and the insertion process is executed. An overview of the experiment process is displayed in Fig 5.

B. Experiment Design

The robot introduced in section 3 is programmed to assemble the bare PCB with IGBT. The assembly time is regarded as the metric for evaluating the efficiency of search methods. All search methods exploited for experiments include:

- (1) **Line Search:** The robot implements the linear search method solely and performs a search for the insertion hole along a predefined direction to guarantee the holes can be consistently located after multiple attempts.
- (2) **Spiral Search:** The robot implements the spiral search method with the initial point optimization. In this circumstance, the robot performs a search along a spiral path.

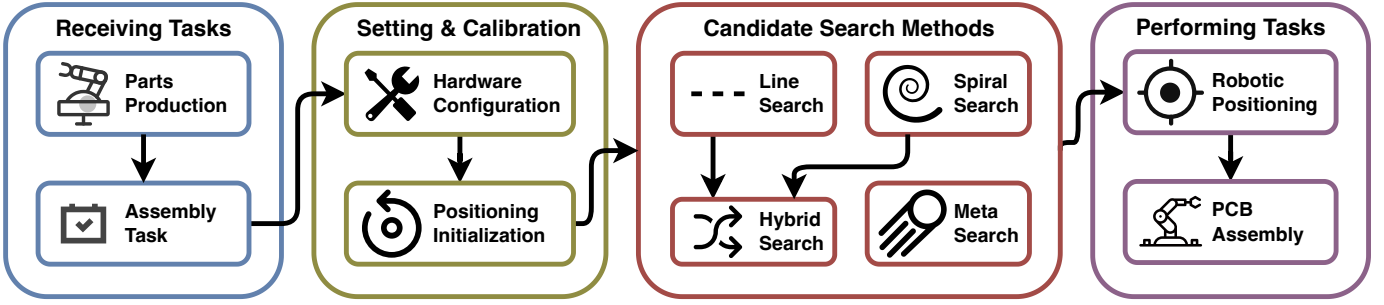


Fig. 5. The overview experiment process.

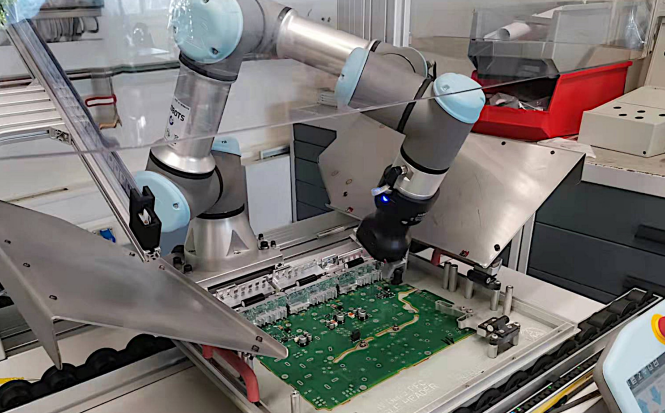


Fig. 6. The assembly unit with one IGBT component.

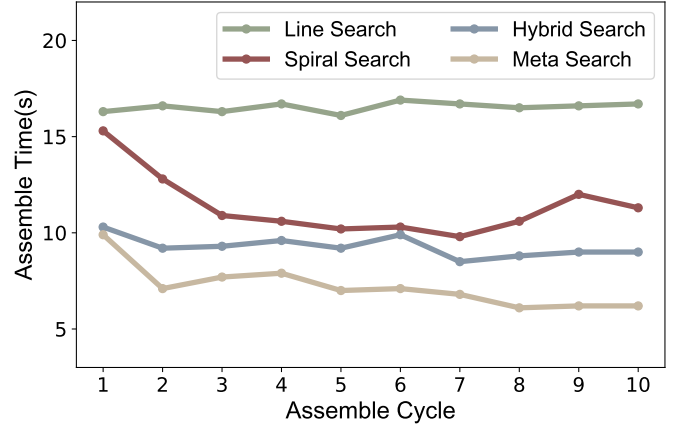


Fig. 7. Assemble time for abnormal position.

(3) **Hybrid Search:** The robot alternately performs a one-step line search and then a one-step spiral search.

(4) **Meta Search:** The robot assembles the PCB by implementing the proposed meta search method.

For each experiment, the robot performs continuous assembly of **10** different PCBs of the same type. In each individual PCB, a total of **9** IGBTs are required to be inserted. The assembly process is concluded when the insertion hole is successfully located or the maximum allotted search time has been reached. It is worth noting that the **7th** hole position in each PCB is abnormal due to errors in the manufacturing process of the PCBs. The line search method, spiral search method, and hybrid search method necessitate optimizing the initial point before operating each cycle. More precisely, these methods leverage an average approach prior to each cycle, implying that for these three search methods, the starting point for each assembly cycle is computed as the mean of all preceding positions. Contrastingly, the meta search method operates under the assumption that the insertion holes follow a Gaussian distribution, which is continually updated. As a result, there is no need for additional computations to determine the initial position, presenting an inherent advantage of the meta search method.

C. Overall Performance

We evaluate the performance of the proposed methodology in a realistic robotic assembly setup and compare it with other search methods. The results of the experiment are listed in Table I, which indicated that the proposed meta

method performs better with the minimum assembly time. The meta search method perceives assembly positions as Gaussian distribution, allowing for parameters updated during the subsequent assembly process, which suggests that the meta method is inherently a "learning method." Consequently, the assembly process accelerates alongside the progression of the experiment. Comparable results are observed for both the spiral and hybrid search methods, as they can progressively locate the optimized initial point throughout the experimental progression. Regarding the linear search, the assembly process did not show an increase in speed throughout the experimental procedure. This is due to the fact that the linear search is limited to rectifying errors solely in the direction of the search line. Thus, the actual assembly position cannot be identified effectively once it deviates from the linear path.

D. Study of self-adaption ability

In this section, the self-adaption ability of the search method is studied. Specifically, the **7th** hole position within each PCB is considered abnormal due to its more discrete distribution. To assess the self-adaptation capability, the assembly time for the 7th hole within each PCB is particularly recorded and evaluated. The experimental results are shown in Fig. 7. In the case of the line search method, the assembly time remains consistently high, indicating a subpar ability to adapt to such abnormal assembly positions. Conversely, both the spiral search and hybrid search methods exhibit an increase in assembly speed as the experiment progresses. This improvement can be attributed to exploiting the average approach,

TABLE I
COMPARISON OF POSITIONING ABILITY FOR ASSEMBLE TASK.

Method	Assemble Cycle Time(s)										Average Assemble Time
	C1	C2	C3	C4	C5	C6	C7	C8	C9	C10	
Line Search	106.2	105.2	106.0	106.9	107.7	104.8	109.2	108.5	105.6	109.1	106.6
Spiral Search	102.7	72.1	64.6	58.3	62.8	60.4	63.8	59.9	57.3	61.1	66.0
Hybrid Search	78.1	64.8	62.6	63.6	60.8	61.5	59.2	57.7	56.8	58.5	62.3
Meta Search	73.5	48.8	40.9	40.3	42.0	38.7	36.4	36.6	37.7	35.6	42.6

which provides a rough yet restricted search range, thereby augmenting the assembly speed during subsequent processes. The meta search method achieves the best performance in this scenario, signifying its superior ability to adapt to such abnormal positions, which indicates that the meta method can deal with complex situations, such as cases where the holes are irregular (e.g., the holes in the shapes of ellipses).

E. Study of regularization factor

In this section, we explore the effect of regularization factor Λ in Eq.36 and Eq.37, which controls the punishment between different candidate assemble positions during meta search method. The assembly process with and without regularization are compared and illustrated at Fig 8. For the meta search method without regularization, obvious overlaps exist between candidate assembly positions, resulting in a significant decrease in assembly speed. This clearly demonstrates the need for regularization when employing the meta search method. After that, the explicit effect of the regularization factor λ is well studied as an ablation experiment. The average assembly time for ten different PCBs is regarded as the metric. The experiment result is listed in Table II

TABLE II
ABLATION STUDY OF REGULARIZATION FACTOR λ

Regularization Fator λ	$1e^{-2}$	$1e^{-3}$	$1e^{-4}$	$1e^{-5}$	$1e^{-6}$
Average Assemble Time(s)	89.4	85.2	42.5	56.9	72.5

The experimental result remains consistent with the theoretical analysis. A much too high λ will bring divergence; meanwhile, a much too low λ will still lead to collapse. Hence, the regularization factor λ is fixed as $1e^{-4}$ as the optimal.

VI. CONCLUSIONS AND FUTURE WORK

In this work, a novel meta search method for precise robotic positioning was proposed, which has self-learning ability and can be adapted for new assembly tasks under constrained environments that are unsuitable for integrating the vision system. The effectiveness, as well as the self-adaption ability of this method, is demonstrated by conducting experiments in a real robot assembly environment. It is hoped that this approach will inspire researchers studying robotic positioning, and researchers are highly recommended to consider extending this component-agnostic method to other application areas.

There exist two interesting future research directions: **Robotic positioning for the deformable component.** Robotic positioning for deformable is a frequently encountered working scenario characterized by the challenge of the components being prone to damage. When numerous assembly attempts are made, the assembly process will be hindered by the deformation of these components. Enhancing the proposed meta search method would be highly beneficial in enabling its application in this particular scenario. **Dynamic robotic positioning for the movable component.** When enhancements are made to the meta algorithm in dynamic positioning, allowing it to adapt to the target object's motion trajectory accurately while

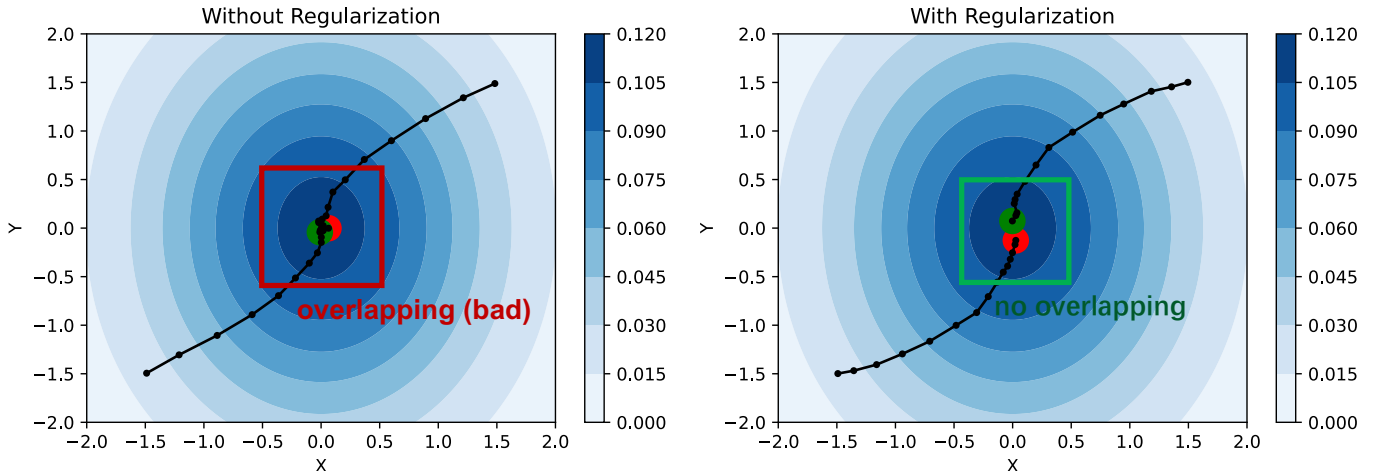


Fig. 8. Search the cover(s) of maximum probability (**Left:** search without regularization and **Right:** search with regularization). Notice that without any regularization the covers will tend to collapse.

compensating for positioning errors, the method will make a remarkable contribution to flexible manufacturing.

ACKNOWLEDGMENTS

This arXiv manuscript reflects the original agreed version. Dr. Teng conducted independent research, solely authored **Algorithm 2, Sections III.A, III.C and V.E** in their entirety, and created all associated figures. Misuse is evident in both the journal (*DOI:10.1016/j.jmsy.2024.11.009*) and the patent (*CN 118960772 A*). His contributions to the paper were strictly confined to **meta method design, theoretical analysis, and writing/revision of the overall paper**, with no involvement beyond these declared aspects.

The other parts of the work were partially supported by National Key R&D Program of China (No.2017YFE0101400), National Key R&D Program of China with Grant number 2018YFB1800804, the National Natural Science Foundation of China (Nos. NSFC 61925105, and 62171257) and Tsinghua University-China Mobile Communications Group Co., EU H2020 Research and Innovation Program under the Marie Skłodowska-Curie Grant Agreement (Project-DEEP).

This declaration has been reviewed and acknowledged by **Tsinghua University's Academic Committee** and serves as an authoritative reference regarding Dr. Teng's contributions.

REFERENCES

- [1] K. Kimble, K. Van Wyk, J. Falco, E. Messina, Y. Sun, M. Shibata, W. Uemura, and Y. Yokokohji, "Benchmarking protocols for evaluating small parts robotic assembly systems," *IEEE robotics and automation letters*, vol. 5, no. 2, pp. 883–889, 2020.
- [2] H. Xie, W.-l. Li, D.-H. Zhu, Z.-p. Yin, and H. Ding, "A systematic model of machining error reduction in robotic grinding," *IEEE/ASME Transactions on Mechatronics*, vol. 25, no. 6, pp. 2961–2972, 2020.
- [3] E. Colleoni, P. Edwards, and D. Stoyanov, "Synthetic and real inputs for tool segmentation in robotic surgery," in *Medical Image Computing and Computer Assisted Intervention—MICCAI 2020: 23rd International Conference, Lima, Peru, October 4–8, 2020, Proceedings, Part III 23*. Springer, 2020, pp. 700–710.
- [4] W.-C. So, C.-H. Cheng, W.-Y. Lam, T. Wong, W.-W. Law, Y. Huang, K.-C. Ng, H.-C. Tung, and W. Wong, "Robot-based play-drama intervention may improve the narrative abilities of chinese-speaking preschoolers with autism spectrum disorder," *Research in developmental disabilities*, vol. 95, p. 103515, 2019.
- [5] Y. Zeng, W. Tian, and W. Liao, "Positional error similarity analysis for error compensation of industrial robots," *Robotics and Computer-Integrated Manufacturing*, vol. 42, pp. 113–120, 2016.
- [6] X. Xiao, H. Gao, C. Li, L. Qiu, K. S. Kumar, C. J. Cai, B. S. Bhola, N. K. K. King, and H. Ren, "Portable body-attached positioning mechanism toward robotic needle intervention," *IEEE/ASME Transactions on Mechatronics*, vol. 25, no. 2, pp. 1105–1116, 2020.
- [7] M. Zhang, X. Liu, D. Xu, Z. Cao, and J. Yu, "Vision-based target-following guider for mobile robot," *IEEE Transactions on Industrial Electronics*, vol. 66, no. 12, pp. 9360–9371, 2019.
- [8] T. Lei, Y. Rong, H. Wang, Y. Huang, and M. Li, "A review of vision-aided robotic welding," *Computers in Industry*, vol. 123, p. 103326, 2020.
- [9] Y. Xu, C. Ding, X. Shu, K. Gui, Y. Bezsudnova, X. Sheng, and D. Zhang, "Shared control of a robotic arm using non-invasive brain-computer interface and computer vision guidance," *Robotics and Autonomous Systems*, vol. 115, pp. 121–129, 2019.
- [10] H.-N. Nguyen, P.-N. Le, and H.-J. Kang, "A new calibration method for enhancing robot position accuracy by combining a robot model-based identification approach and an artificial neural network-based error compensation technique," *Advances in Mechanical Engineering*, vol. 11, no. 1, p. 1687814018822935, 2019.
- [11] W. Zhu, G. Li, H. Dong, and Y. Ke, "Positioning error compensation on two-dimensional manifold for robotic machining," *Robotics and Computer-Integrated Manufacturing*, vol. 59, pp. 394–405, 2019.
- [12] V. Chauhan and B. Surgenor, "A comparative study of machine vision based methods for fault detection in an automated assembly machine," *procedia manufacturing*, vol. 1, pp. 416–428, 2015.
- [13] D. De Gregorio, R. Zanella, G. Palli, S. Pirozzi, and C. Melchiorri, "Integration of robotic vision and tactile sensing for wire-terminal insertion tasks," *IEEE Transactions on Automation Science and Engineering*, vol. 16, no. 2, pp. 585–598, 2019.
- [14] H. Nakagaki, K. Kitagaki, T. Ogasawara, and H. Tsukune, "Study of deformation and insertion tasks of a flexible wire," in *Proceedings of International Conference on Robotics and Automation*, vol. 3, 1997, pp. 2397–2402 vol.3.
- [15] C. Feng, Y. Xiao, A. Willette, W. McGee, and V. R. Kamat, "Vision guided autonomous robotic assembly and as-built scanning on unstructured construction sites," *Automation in Construction*, vol. 59, pp. 128–138, 2015.
- [16] Z. Qin, P. Wang, J. Sun, J. Lu, and H. Qiao, "Precise robotic assembly for large-scale objects based on automatic guidance and alignment," *IEEE Transactions on Instrumentation and Measurement*, vol. 65, no. 6, pp. 1398–1411, 2016.
- [17] W. Wan, F. Lu, Z. Wu, and K. Harada, "Teaching robots to do object assembly using multi-modal 3d vision," *Neurocomputing*, vol. 259, pp. 85–93, 2017.
- [18] W.-C. Chang, "Robotic assembly of smartphone back shells with eye-in-hand visual servoing," *Robotics and Computer-Integrated Manufacturing*, vol. 50, pp. 102–113, 2018.
- [19] H. Cheng, H. Chen, L. Hao, and W. Li, "Robot learning based on partial observable markov decision process in unstructured environment," in *2014 IEEE International Conference on Robotics and Automation (ICRA)*. IEEE, 2014, pp. 4399–4404.
- [20] G. Fontana, S. Ruggeri, I. Fassi, and G. Legnani, "A mini work-cell for handling and assembling microcomponents," *Assembly Automation*, 2014.
- [21] Y. Lin, Y. Li, Y. Huang, K. Zhang, H. Zhu, Y. Liu, and Y. Guan, "An odd-form electronic component insertion system based on dual scara," in *2018 IEEE International Conference on Robotics and Biomimetics (ROBIO)*. IEEE, 2018, pp. 1514–1520.
- [22] K. Zhang, Y. Li, Y. Guan, L. He, Y. Gan, and Z. Dong, "A vision detection system for odd-form components," in *2018 IEEE International Conference on Robotics and Biomimetics (ROBIO)*. IEEE, 2018, pp. 120–125.
- [23] J. Liang, G. Ye, J. Li, Y. Kuang, and X. Zhang, "Pose alignment for electronic component insertion using rotational stereo vision," in *2018 IEEE International Conference on Robotics and Biomimetics (ROBIO)*. IEEE, 2018, pp. 2421–2427.
- [24] W. Liu, W. Chen, and R. Wu, "Lsd based vision detection system for industrial robot under complex illumination conditions," in *2019 IEEE International Conference on Robotics and Biomimetics (ROBIO)*. IEEE, 2019, pp. 30–35.
- [25] P. Nerakae, P. Uangpairaj, and K. Chamniprasart, "Using machine vision for flexible automatic assembly system," *Procedia Computer Science*, vol. 96, pp. 428–435, 2016.
- [26] S. Chhatpar and M. Branicky, "Localization for robotic assemblies with position uncertainty," in *Proceedings 2003 IEEE/RSJ International Conference on Intelligent Robots and Systems (IROS 2003) (Cat. No.03CH37453)*, vol. 3, 2003, pp. 2534–2540 vol.3.
- [27] E. Langetepe, "On the optimality of spiral search," in *Proceedings of the twenty-first annual ACM-SIAM symposium on Discrete Algorithms*. SIAM, 2010, pp. 1–12.
- [28] I. Al-Nahhal, O. A. Dobre, E. Basar, C. Moloney, and S. Ikki, "A fast, accurate, and separable method for fitting a gaussian function [tips & tricks]," *IEEE Signal Processing Magazine*, vol. 36, no. 6, pp. 157–163, 2019.
- [29] S. Balduzzi, G. Rücker, and G. Schwarzer, "How to perform a meta-analysis with r: a practical tutorial," *BMJ Ment Health*, vol. 22, no. 4, pp. 153–160, 2019.
- [30] Y. Cohen, H. Naseraldin, A. Chaudhuri, and F. Pilati, "Assembly systems in industry 4.0 era: a road map to understand assembly 4.0," *The International Journal of Advanced Manufacturing Technology*, vol. 105, pp. 4037–4054, 2019.